

1

2

3 Endocytosis caused by liquid-liquid phase separation of proteins

4

5 Louis-Philippe Bergeron-Sandoval¹, Hossein Khadivi Heris², Catherine Chang³, Caitlin E.
6 Cornell³, Sarah L. Keller³, Paul François⁴, Adam G. Hendricks², Allen J. Ehrlicher², Rohit V.
7 Pappu⁵ and Stephen W. Michnick^{1,6*}

8 Affiliations

9 †Département de Biochimie, Université de Montréal, C.P. 6128, Succursale centre-ville, Montréal, Québec,
10 H3C 3J7, Canada.

11 ‡Department of Bioengineering, McGill University, 817 Sherbrooke St West, Room 270, Montreal, Quebec,
12 H3A 0C3, Canada.

13 †Department of Chemistry, University of Washington, Seattle, Seattle WA 98195-1700 USA

14 †Ernest Rutherford Physics Building, McGill University, 3600 University St, Montreal, Québec, H3A 2T8

15 †Department of Biomedical Engineering and Center for Biological Systems Engineering, Washington
16 University in St. Louis, One Brookings Drive, Campus Box 1097, St. Louis, Missouri 63130, USA.

17 †Centre Robert-Cedergren, Bio-Informatique et Génomique, Université de Montréal, C.P. 6128, Succursale
18 centre-ville, Montréal, Québec, H3C 3J7, Canada.

19

20 *Correspondence to: S.W.M. (stephen.michnick@umontreal.ca).

21

22 Summary

23

24 Endocytosis underlies intra- and extracellular material trafficking in eukaryotes, and is essential to
25 protein metabolism, intercellular signaling, membrane remodeling and other cell regulatory
26 processes. Although endocytosis is usually driven by F-actin polymerization in yeast cells,
27 membrane invagination can also occur through a yet unknown actin-independent mechanism when
28 turgor pressure is relieved. Here, we demonstrate that membrane invagination can arise from
29 liquid-liquid phase separation (demixing) of proteins with prion-like domains (PLD) from the
30 cytosol. Demixing of these proteins results in the formation of a protein condensate, which, by
31 virtue of its composition and viscoelastic properties, binds to and deforms plasma membrane and
32 cytosol. Demonstration that phase separated condensates can perform mechanical work expands
33 the repertoire of known functions of protein condensates to include the ability to do work at soft
34 interfaces such as between the condensate and the membrane. Similar mechanisms may govern or
35 contribute to other membrane shaping, invagination and budding processes that are involved in
36 cellular material uptake, secretion, and cell shape remodeling.

37 Introduction

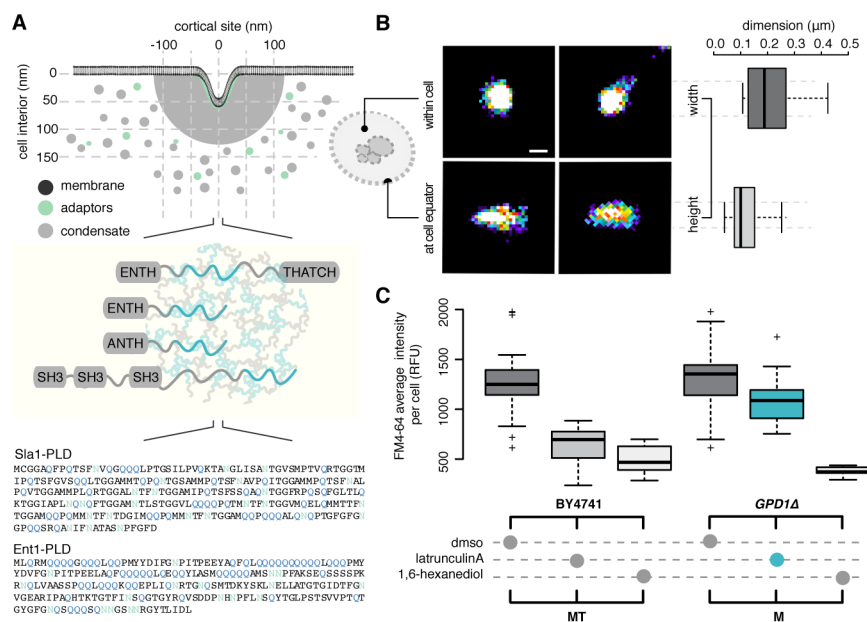
38 Evolution has resulted in numerous innovations by which morphogenesis of organisms
39 occurs within limits imposed by physical and chemical constraints (Darwin 1859, Thompson
40 1917). One such process is clathrin-mediated endocytosis (CME) a fundamental mechanism of
41 cell surface membrane receptor turnover and recycling, nutrient uptake and synaptic vesicle
42 regeneration, among others (Conner and Schmid 2003). The mechanism of membrane invagination
43 through endocytosis in budding yeast cells has most convincingly been demonstrated to be growth
44 of membrane-bound branched actin (Skruzny, Brach et al. 2012), although the term “CME” has
45 historically been retained. When actin is polymerized, it bundles into an active gel with mechanical
46 properties that facilitate endocytosis at localized sites (Carlsson and Bayly 2014, Weirich,
47 Banerjee et al. 2017). However, CME has also been shown to occur under conditions where actin
48 polymerization is absent in both yeast and mammalian cells (Aghamohammadzadeh and Ayscough
49 2009, Basu, Munteanu et al. 2014, Li, Shao et al. 2015).

50
51 The contribution of actin polymerization to CME in mammalian cells is ambiguous, since equal
52 population of clathrin-coated pits mature into vesicles either with or without the need for cortical
53 filamentous actin at endocytic sites (Li, Shao et al. 2015). In the budding yeast *S. cerevisiae*, the
54 dominant mechanism for vesicle generation in CME is branched actin assembly, which is required
55 to compete against intracellular turgor pressure and membrane tension to drive the invagination of
56 the plasma membrane (Carlsson and Bayly 2014). If, however, turgor pressure is eliminated in
57 yeast cells, CME can also occur, independent of actin polymerization (Aghamohammadzadeh and
58 Ayscough 2009). A similar phenomenon has been observed in fission yeast (Basu, Munteanu et
59 al. 2014). Several mechanisms that could explain actin-independent membrane invagination in
60 CME have been proposed (see Discussion) but individual or combined contributions of these
61 mechanisms to CME *in vivo* remain unclear.

62
63 Here, we present evidence for a novel mechanism of actin-independent CME in a yeast cell mutant
64 model in which turgor pressure is relieved and actin polymerization is specifically inhibited
65 (Figure 1A and S1). This mechanism was suggested to us by the observation that there is a common
66 intrinsically disordered amino acid sequence pattern called prion-like domains (PLD) found among
67 coat and adapter proteins Sla1/2, Ent1/2 and Yap1801/2 (Figure 1A) (Alberti, Halfmann et al.
68 2009, Malinowska, Kroschwald et al. 2013). PLD-containing proteins are known to phase separate
69 *in vitro* and in cells and interact through amino acid sequence motifs found within the PLDs
70 (Alberti, Saha et al. 2018, Wang, Choi et al. 2018). Phase separation leads to spherical condensates
71 that are hundreds of nanometers to micrometers in size with a range of viscoelastic properties
72 (Pappu, Wang et al. 2008, Brangwynne, Eckmann et al. 2009, Kroschwald, Maharana et al. 2015,
73 Molliex, Temirov et al. 2015, Wang, Choi et al. 2018). Nucleation and growth of such condensates
74 within cells has the potential to deform the cytosol and other elastic structures found inside these
75 cells (Style, Sai et al. 2018). It has also been demonstrated that membranes can be deformed *in*
76 *vitro* by liquid-liquid phase separation of polymer condensates (Li, Lipowsky et al. 2011).

77
78
79
80
81
82
83
84
85

We postulate that such condensates exist at CME initiation sites and that, owing to their viscoelastic properties and interfacial tension, bind to the plasma membrane adaptors and generate force to drive invagination of the membrane (Figure 1A). This model can implicitly include and integrate the contributions of the previously proposed mechanisms for membrane invagination in actin-independent CME (detailed in the Discussion). Notably, our model explains how proteins are concentrated at endocytic sites to bind to and alter the properties or composition of the membrane, such that elastic resistance of the membrane to deformation is reduced.



86
87
88
89
90
91
92
93
94
95
96
97
98
99
100
101
102
103
104
105
106
107

Figure 1 | Phase-separation of proteins into an endocytic condensate can drive clathrin-mediated endocytosis (A) (Upper panel) Illustration of the geometry of a plasma membrane (dark grey) invagination into the cell during clathrin-mediated endocytosis (CME). Electron microscopic data suggest that clathrin-coated plasma membrane patches are surrounded by a cortical body of ~ 200 nm diameter (light grey) before appearance of actin structures. Clathrin heavy and light chains (Chc1 and Clc1) interact with adaptor proteins (Ede1 and Syp1) to form a lattice on the membrane (in green). Subsequently, early coat proteins (light grey), such as Sla1/2, Ent1/2, and Yap1801/2, directly bind to the adaptor-clathrin lattice and form the endocytic condensate (in grey). (middle panel) Coat proteins Sla1/2, Ent1/2 and Yap1801/2 contain “Prion-like domains” (PLD, in blue) that include tandem repeats of asparagine and glutamine. (lower panel) Examples of PLD sequences from Sla1 and Ent1 (B) Geometry and size distribution of coat protein Sla1-GFP at cortical sites measured using super-resolution microscopy (dSTORM). Lateral x, y resolution was ~ 10 nm. Pseudo-color reconstructed images show circular structures (left panels) when viewed from the top, or within cells (left, upper), but form narrow ellipses when imaged at the equator of cells (left, lower). Automatic segmentation and morphological analysis (right panels) were performed on these reconstructed images to determine the width (209 ± 10 nm) and height (118 ± 6 nm) of cortical bodies (mean \pm sd; $n = 250$), consistent with other electron and light micrographic evidence. (C) Lipophilic cargo membrane-labelling dye FM4-64 is taken up into vesicles by CME in wild type BY4741 (left) and *GPD1* Δ cells (eliminates turgor pressure; right) treated with either DMSO, latrunculin A (prevents F-actin polymerization) or 1,6-hexanediol (disrupts liquid-liquid phase separated protein condensates). Each boxplot (center line, median; box, upper and lower quartiles; whiskers, 1.5x IQR; crosses, outliers) shows

108 the relative fluorescence units of $n = 50$ cells. Note that *GPD1* Δ cells can undergo CME in the absence of
109 F-actin polymerization (blue) because there is no turgor pressure in these cells. See also Figure S1.

110

111 **PLD-containing CME proteins phase-separate into protein condensates**

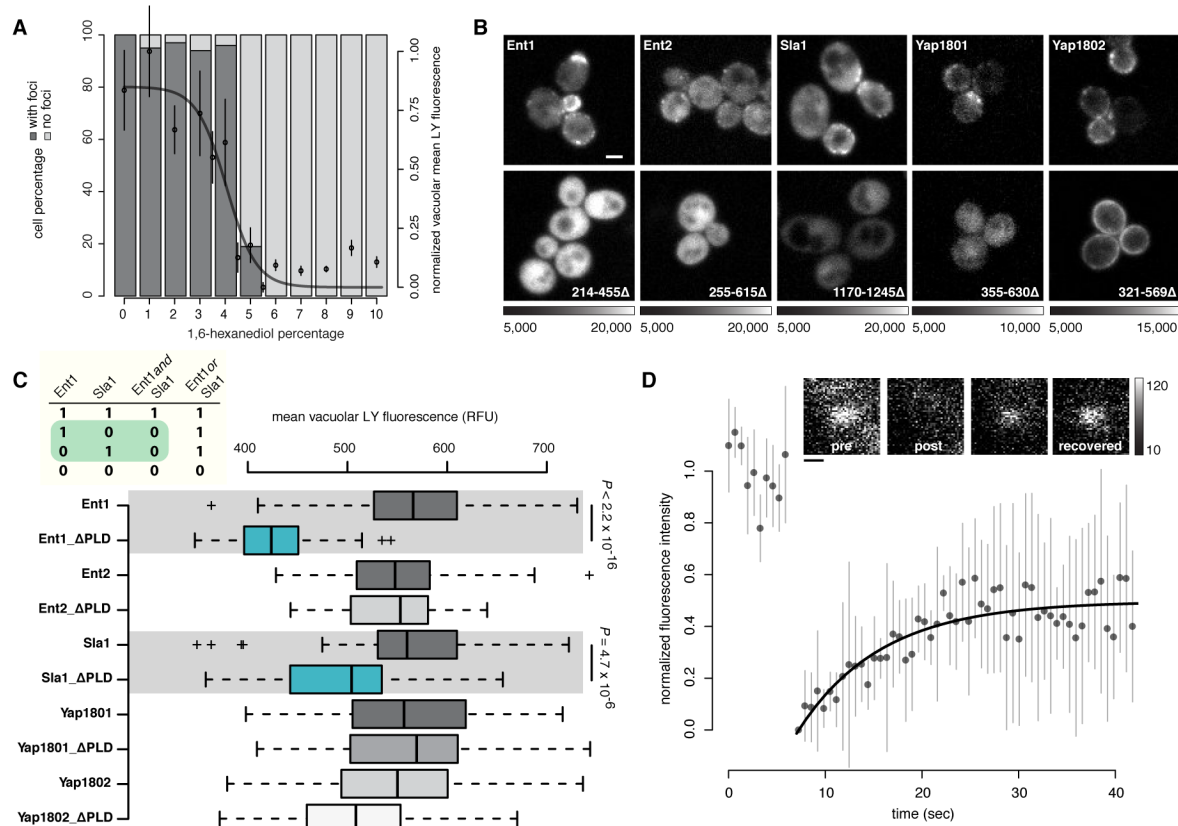
112

113 We first observed protein puncta that form at cortical sites of 209 ± 10 nm diameter and 118 ± 6
114 nm height by super-resolution fluorescence imaging of the PLD-containing endocytic coat protein
115 Sla1 in *GPD1* Δ cells treated with Latrunculin A (Lat A), an inhibitor of actin polymerization
116 (Figure 1B and S1). Our data, which are similar to reported measures of Sla1 high resolution
117 structures (Mund, van der Beek et al. 2017), indicate that Sla1 assembles into a dome-shaped
118 structure under the conditions that we performed these experiments, consistent with a protein
119 condensate (henceforth called the endocytic condensate) that associates with the membrane on
120 cortical sites. Other existing evidence that a protein condensate could exist at CME sites include
121 electron and light microscopic studies that reveal a region surrounding CME membrane
122 invaginations of ~ 200 nm diameter that are devoid of ribosomes. Furthermore, before actin
123 polymerization is initiated (as visualized by fluorescent protein-tagged Apb1) these “ribosome-
124 free zones” are also observed on most sites (75%) suggesting that these zones can be composed of
125 coat proteins (as visualized by fluorescent protein-tagged Sla1) and do not contain polymerized
126 actin (Kukulski, Schorb et al. 2012). Sla1-labelled condensates thus appear to present a physical
127 barrier to large molecular complexes, at least as large as ribosomes (> 25 nm). We next performed
128 a series of experiments to establish that endocytic puncta are phase-separated protein condensates
129 and we probed their properties and permeability.

130

131 The simple alcohol 1,6-hexanediol (HD) has been demonstrated to prevent liquid-liquid phase
132 separation of proteins *in vivo* and *in vitro* (Updike, Hachey et al. 2011, Kroschwald, Maharana et
133 al. 2015, Molliex, Temirov et al. 2015). CME, as measured by cell uptake of a lipophilic
134 membrane-bound fluorescent dye (FM4-64), was inhibited by HD, whether or not turgor pressure
135 and actin polymerization were present (Figure 1C, left *versus* right panels, respectively).
136 Furthermore, HD prevented uptake of the fluorescent dye Lucifer Yellow (LY) into vacuoles and
137 formation of puncta monitored as Sla1-GFP fluorescence at cortical sites in a dose-dependent
138 manner. No effect was observed in cells treated with the related alcohol 1,2,3-hexanetriol that does
139 not disrupt condensates (Figure 2A and S2A). The other PLD-containing proteins, including Sla2,
140 Ent1, Ent2, Yap1801 and Yap1802, all failed to form puncta in cells treated with HD (Figure S2A).
141 Pulse-chase experiments showed that HD-dependent dissolution of Sla1 puncta was reversible
142 (Figure S2B and Movie S1). In controls, we found 5% HD has no major effect on the integrity of
143 lipid vesicles containing carboxyfluorescein as an indicator of leakage (Figure S2C-E).

144



145
146
147
148
149
150
151
152
153
154
155
156
157
158
159
160
161
162
163
164
165
166
167
168
169
170

Figure 2 | CME adaptor and coat proteins phase separate to form condensates (A) 1,6-hexanediol (HD), disrupts endocytic condensates in an all-or-none manner. Barplot shows percentage of cells that contain Sla1-GFP foci (dark grey), or not (light grey), as a function of HD concentration monitored by counting fluorescent puncta containing Sla1-GFP at cortical sites 5 minutes after HD treatment ($n = 150$ cells). Plot overlay (in black) shows quantification of lucifer yellow fluorescent dye uptake in CME vesicles (mean \pm sd; $n = 25$ foci; logistic fit) (B) Prion-like domains (PLDs) are essential for localization of proteins to the cortical sites. Fluorescence images of cortical localization of Ent1, Ent2, Sla1, Yap1801 and Yap1802 fused to Venus YFP. Localization of full-length (upper panels) *versus* C-terminal PLD truncation mutants of the proteins (lower panels). Amino acid positions of the deleted PLDs are indicated for respective images. Grayscale dynamic range for image pairs are indicated below. Scale bar, 2 μ m. (C) Quantification (box center line, median; box limits, upper and lower quartiles; whiskers, 1.5x IQR; crosses, outliers) by fluorescence microscopy of lucifer yellow dye uptake for strains that express either full-length or PLD-truncated Ent1, Ent2, Yap1801, Yap1802 and Sla1 (as detailed in panel b). We observed a significant decrease in CME for PLD truncation mutants of Sla1 and Ent1 ($n = 100$ cells; two-sided t-test; see Methods). Presence (1) or absence (0) of the PLDs of either Ent1 or Sla1 are the input variables in the truth table (top insert; values that we determined in green). (D) Coat proteins exchange with endocytic condensates at rates typical of those observed for proteins that compose other protein condensates. Fluorescence recovery after photo bleaching (FRAP) of Sla1-GFP, GFP signal recovery was measured within a segmented Sla1-mCherry region of interest to ensure that FRAP was acquired within the endocytic condensate (mean \pm sd; $n = 10$ cells. Data was fitted to a single term recovery equation) (Methods). Incomplete fluorescence recovery suggests that endocytic condensates are viscoelastic. Representative foci images before bleaching, upon bleaching, and after recovery are shown in inserts. 8-bit grayscale values, 10 to 120. Scale bar, 250 nm. See also Figure S2.

171 Alberti *et al.* reported that PLDs of Sla1/2, Ent1/2 and Yap1801/2 all form puncta individually,
172 without amyloid fibril structures, as probed by binding to Thioflavin T (ThT) (Khurana, Coleman
173 *et al.* 2005, Alberti, Halfmann *et al.* 2009). Consistent with the behavior of these PLD fragments
174 and formation of non-amyloid condensates, we observed no colocalization of ThT with Sla1-
175 mCherry-labelled puncta (Figure S2F-G).

176
177 We observed that the PLDs of CME coat proteins were essential to their localization to cortical
178 sites (Figure 2B). Furthermore, CME was significantly reduced in cells where the PLDs of Sla1
179 and Ent1 were deleted and with substitutions of proline for other residues in the Sla1 PLD, which
180 weakens the driving force for phase separation (Figure 2C and S2H) (Toombs, McCarty *et al.*
181 2009, Peskett, Rau *et al.* 2018). Our results are consistent with previous reports of the mis-
182 localization of the N-terminal SH3 domains of Sla1 (Warren, Andrews *et al.* 2002) and of the Ent2
183 ENTH2 domain (Mukherjee, Coon *et al.* 2009). They are also consistent with disruption of CME
184 resulting from deletion of the Sla1 C-terminal region (Warren, Andrews *et al.* 2002). While some
185 functional redundancy is possible among the PLD-containing coat proteins, the two that are most
186 essential, Sla1 and Ent1, are both required for specific protein-protein interactions and/or functions
187 mediated by other domains within their sequences.

188
189 The interactions among proteins in liquid-liquid phase separated condensates are expected to be
190 weak (Li, Chavali *et al.* 2018), explaining their rapid exchange within and between condensates
191 and their surroundings (Brangwynne, Eickmann *et al.* 2009, Lin, Protter *et al.* 2015, Feric, Vaidya
192 *et al.* 2016). In fluorescence recovery after photobleaching (FRAP) experiments we measured
193 equivalent mobile and immobile fractions (0.50 ± 0.02 ; mean \pm sem) for the protein Sla2 (Figure
194 2E), similar to other protein and nucleic acid condensates including the dense internal fibrillar
195 component of *X. laevis* nucleoli (Feric, Vaidya *et al.* 2016). We acquired recovery traces when the
196 apparent number of Sla2 molecules in the fluorescent foci remains relatively constant (pre-bleach
197 intensities do not increase in Figure 2E).

198

199 **Condensation is required for CME protein-protein interactions and endocytosis**

200

201 The regulation of CME involves the dynamic assembly of a protein-protein interaction network
202 through mostly transient and weak protein-protein interactions (Boeke, Trautmann *et al.* 2014).
203 This observation begs a subtle and important question: Is the formation of the protein-protein
204 interaction network the result of phase separation into condensates or do endocytic condensates
205 reflect the formation of an obligate and fixed protein-protein interaction network? One could
206 argue, for instance, that deletion of the PLDs of Sla1 and Ent1 prevents membrane invagination
207 and therefore endocytosis by virtue of removal of binding motifs in the PLDs required for
208 interactions of both of these proteins (Figure 2B-C). It could even be argued that the subtle proline
209 substitution mutations in the Sla1 PLD inhibit CME because they prevent protein-protein

210 interactions by disrupting alpha-helical structural motifs essential for the protein-protein
211 interactions of Sla1 (Figure S2H).

212

213 We distinguish these two possibilities based on simple logic as formally introduced in a truth table
214 (Figure 3A, D): If the PLDs of Ent1 and Sla1 are *both* required for forming protein-protein
215 interactions essential for CME then we *cannot* substitute the PLD of one for the other. If, however,
216 we can substitute one PLD for the other and recover both phase separation and CME function, then
217 the properties of the PLDs that allow them to phase-separate and allow for endocytosis is important
218 rather than the fixed protein interaction network. A caveat would arise if Sla1 and Ent1 PLDs
219 shared common binding motifs that govern essential protein-protein interactions. We found,
220 however, that Sla1 PLD and Ent1 PLD share low sequence identity (23.6 percent) and the single
221 motif TG(F/Y)GFGN (Figure S3A). More importantly, they share only two protein-protein
222 interactions that are not essential to endocytosis (Chc1 and Ubi4; physical interactions detected by
223 at least two experiments from the BioGRID database).

224

225 Since both Sla1 *and* Ent1 PLD domains are essential for endocytic condensate localization and
226 endocytosis (Figure 2C), we needed to test the essentiality of the PLD of only one of these proteins
227 and therefore chose that of Sla1. We first compared the protein-protein interactions between
228 *wildtype* and the PLD deletion mutant of Sla1 *in vivo* using a Protein-fragment Complementation
229 Assay with the reporter protein DiHydroFolate Reductase (DHFR PCA) (Figure S3B-C). We
230 confirmed 13 potential Sla1 protein-protein interactions selected from *BioGRID* (thebiogrid.org)
231 found amongst membrane adaptors (Chc1, Ede1, End3), PLD-containing coat proteins (Sla1, Sla2,
232 Yap1802), actin polymerization machinery (Arc40, Las17, Lsb3, Ysc84, Abp1) and chaperones
233 (Hsp104, Ssa2). Selection for DHFR reconstitution with Sla1, in which the PLD was deleted (*Sla1*
234 Δ PLD), revealed that all interactions are lost with the exception of 2, Sla2 and Apb1 (Figure S3B-
235 C). The loss of interactions is consistent with yeast two-hybrid studies of Sla1 in which the C-
236 terminal repeats, within our PLD, are deleted resulting in loss of Sla1 protein-protein interactions
237 (Tang, Xu et al. 2000). We observed that phase separation of Sla1 *in vitro* is equivalent after
238 deletion of the PLD while phase separation of Ent1 in which the PLD was deleted (Ent1- Δ PLD)
239 is completely prevented under the same conditions (Figure S3D). We thus conclude that *in vivo*,
240 the PLD of Sla1 is essential for normal CME function and Sla1 protein-protein interactions (Figure
241 2 and S3B-C).

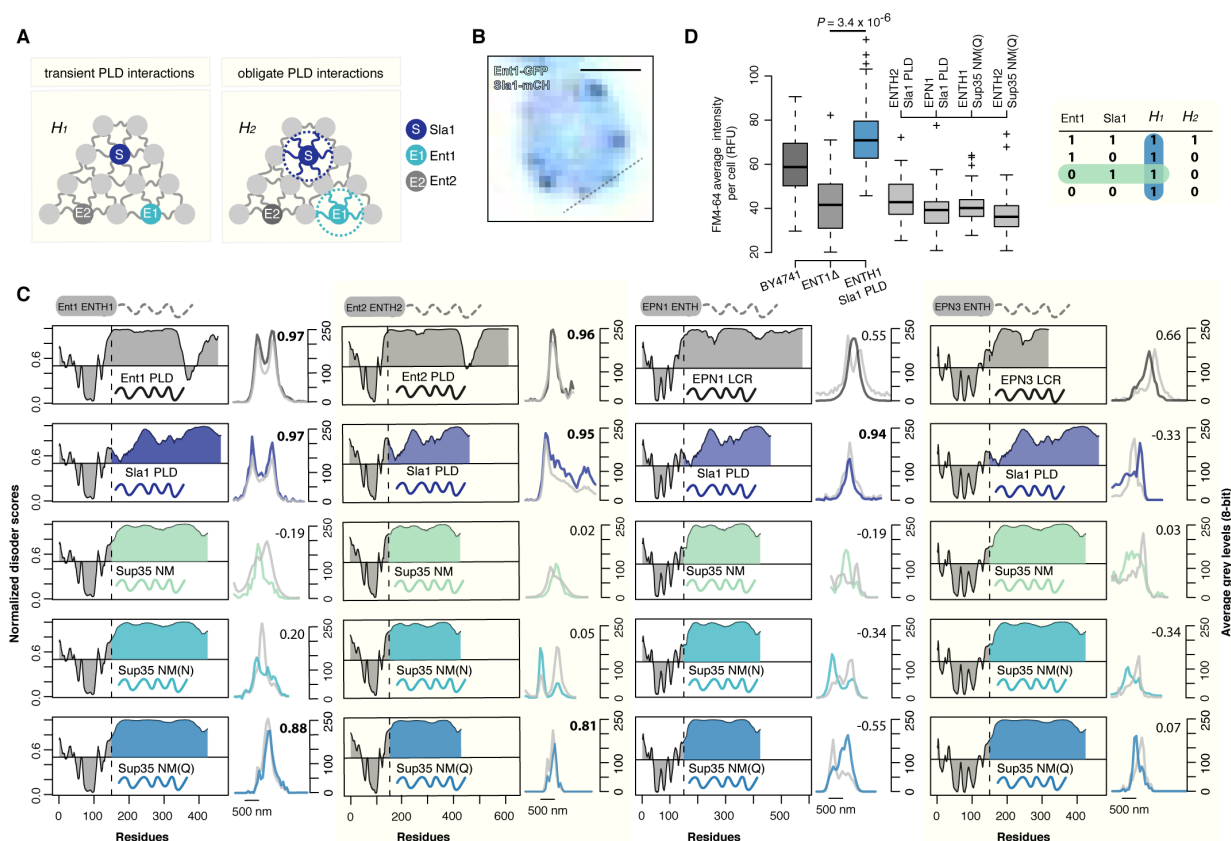
242

243 We next distinguished between the two opposing PLD-driven phase-separation *versus* obligate
244 protein-protein interaction network hypotheses (Figure 3A). We did this by comparing results of
245 phase separation and endocytosis for the substitution of PLD domains in either Ent1 or Sla1.

246

247 We thus engineered two types of chimeric proteins that contain either Sla1 PLD or sequence
248 variants of Sup35 NM fused to N-terminal ENTH region (ENTH1) of yeast Epsin protein Ent1.
249 We included sequence variants of Sup35 NM – a PLD of the classic prion protein Sup35 in which

250 either all asparagine (N) residues are substituted with glutamine (Q) or *vice versa* in the NM
 251 domain, yielding mutants Sup35 NM(Q) and Sup35 NM(N). We chose these sequences for two
 252 reasons. First, Sup35 is the archetypal prion protein used to determine sequence compositions of
 253 all PLDs in the yeast genome. Second, because the mutant Sup35 NM(Q) shares amino acid
 254 composition with Sla1 PLD and both undergo non-nucleation-limited self-assembly (Alberti,
 255 Halfmann et al. 2009, Khan, Kandola et al. 2018). We also engineered chimeric Epsin proteins
 256 from the yeast paralog Ent2 (for which the PLD is essential for phase separation but not for CME
 257 function) and human homologs EPN1/3 as controls (Figure 3C).
 258



259
 260
 261 **Figure 3 | PLDs are interchangeable and modulate assembly of chimeric proteins into phase-**
 262 **separated bodies** (A) Illustration of the hypothesis (H₁) that coat proteins condense together through
 263 transient PLD interactions, and the alternate hypothesis (H₂) that coat proteins assemble into a complex
 264 through obligate protein-protein interactions. (B) Colocalization of Ent1-GFP signal within a Sla1-mCherry
 265 foci in yeast cells, line scan was performed as indicated. Scale bar 1 μM. (C) In the first column, the left
 266 panels show the PDR-fit score (VLS2) for *wildtype* (grey) and chimeric proteins; chimeras include
 267 ENTH1 fused to either Sla1 PLD or Sup35 NM or Sup35 NM(N) or Sup35 NM(Q). Scores above 0.5
 268 indicate the protein region is predicted to be disordered. Right panels show line scans to assess if *wildtype*
 269 or chimeric proteins colocalize with Sla1 foci (grey) in yeast cells. Example of a line scan is given in B.
 270 Pearson correlation values are given to confirm if the signals colocalize. The next columns show the same
 271 analysis for yeast ENTH2, human EPN1 ENTH and human EPN3 ENTH respectively. (D) Quantification
 272 (left panel; box center line, median; box limits, upper and lower quartiles; whiskers, 1.5x IQR; crosses,
 273 outliers) by fluorescence microscopy of FM4-64 dye uptake in cells for strains that overexpress fusions of

274 either Sla1 PLD or Sup35 NM(Qs) to the N-terminal region of yeast Ent1 (ENTH1) or Ent2 (ENTH2)
275 proteins or human EPN1 (ENTH) proteins (n = 100 cells; two-sided t-test; see Methods). Presence of
276 cognate PLD (1) or non-cognate PLD (0) fused to either Ent1 or Sla1 are the input variables in the truth
277 table (right panel). Measures of colocalization and CME levels for ENTH1 Sla1 PLD (green) confirm the
278 hypothesis (*H1*) (blue) that transient PLD interactions drive condensation of coat proteins. See also Figure
279 S3.

280
281 We observed that ENTH1 and ENTH2 domains of Ent1 and Ent2 proteins, respectively fused to
282 either Sla1 PLD or Sup35 NM(Q) localized into- and matured with endocytic condensates (as
283 visualized with Sla1-mCherry) (Figure 3B-C). Absence of colocalization for the other chimeric
284 Epsins suggests that a limited degree of sequence divergence is tolerated for ENTH domains fused
285 to artificial or non-cognate PLDs to partition into endocytic condensates (Figure 3C). Note that
286 Sla1 PLD did, while all Sup35 NM variants did not partition with endocytic condensates on their
287 own (Figure S3E-F). We also observed that the human Epsin homologs EPN1/3 share conserved
288 patterns of disorder with yeast Epsin proteins Ent1/2 (Figure 3C) and thus, we tested whether they
289 would partition with endocytic condensates. We engineered chimeric proteins of EPN1/3 in which
290 their low complexity domains (LCDs) were replaced with either Sla1 PLD or sequence variants of
291 Sup35 NM. Although EPN1 and EPN3 *wildtype* and chimeric constructs all formed foci in yeast
292 cells, only the chimeric EPN1 ENTH fused to the Sla1 PLD localized into- and matured with
293 endocytic condensates (Figure 3C and Figure S3G-I).

294
295 We next tested whether the chimeric Epsins could function by measuring FM4-64 dye uptake in
296 *ENT1Δ* cells (Figure 3D). Only Ent1 ENTH1 domain fused to Sla1 PLD colocalized with
297 endocytic condensates and resulted in recovery of endocytic activity. In controls, we observed no
298 function rescue by other Sla1 PLD fusions (Figure 3D). Thus, we propose that this result is the
299 “exception that disproves the rule” that formation of an obligate protein-protein interaction
300 network by Sla1-PLD is essential for endocytosis to occur. We propose that cognate PLDs mediate
301 phase separation of coat proteins into endocytic condensates (Figure 3D). Additional evidence that
302 goes against the idea that obligate protein-protein interactions underlie coat protein assembly
303 includes the recent observations that coat proteins assemble without perfect stoichiometry of
304 components, unlike the clathrin or Arp2/3 actin complexes (Holland and Johnson 2018). Further,
305 there is no electron micrographic evidence for large protein structures, besides the clathrin mesh,
306 to support the existence of a structured macromolecular complex made of coat proteins (Sochacki,
307 Dickey et al. 2017). Even when actin bundles are present on cortical sites, the actin patches do not
308 have a clear structure and are best described as an active viscoelastic gels (Carlsson and Bayly
309 2014).

310
311 We do not mean to imply that the protein-protein interaction network formed in endocytic
312 condensates is unimportant; evidently it is involved in the regulation of endocytosis. For instance,
313 all of the interactions of coat proteins with the proteins that nucleate actin polymerization are
314 absolutely essential in actin-dependent endocytosis. Our results suggest that in actin-independent
315 endocytosis, phase separation into endocytic condensates is essential for endocytosis and that the

316 formation of the endocytic protein-protein interaction network follows specific PLD-dependent
317 phase separation.

318

319 The observation that the Sup35 NM variants cannot fully complement the Sla1 PLD is consistent
320 with a recent study that uncovered a “molecular grammar” underlying protein liquid-liquid phase
321 separation in so-called FUS family proteins (Wang, Choi et al. 2018). The valency i.e., the numbers
322 of Tyr and Arg residues were shown to be the main determinants of the driving forces for phase
323 separation of FUS family proteins, likely through direct interaction with each other. The authors
324 referred to these residues as “stickers”. The types of residues that are interspersed between Tyr and
325 Arg appear to determine the material properties of condensates. The authors referred to these as
326 “spacers”. Wang *et al.* suggest that the identities of stickers and spacers are likely to be governed
327 by the functions of condensates formed by the IDPs. Indeed, this specificity is manifest in our
328 results that compare the properties of Sup35 NM(Q) mutant to the PLD of Sla1. The amino acid
329 composition of Sup35 NM(Q) mutant is similar to that of Sla1 PLD. However, although this
330 sequence supports phase separation of the chimeria ENTH1::Sup35 NM(Q), it could not support
331 endocytosis (Figure 3C-D). Thus it appears that the PLD sequence of Sla1 and those of other PLD-
332 containing proteins are evolutionarily optimized to enable the formation of endocytic condensates
333 with properties that will give the resulting condensate the properties optimal to drive membrane
334 invaginations.

335

336 Taken together, the totality of our results support the hypothesis that the cortical bodies we study
337 here are phase-separated viscoelastic condensates. We next determined the material properties of
338 the endocytic condensates and tested our postulate that their interactions with the plasma
339 membrane generates the force that drives invagination of the membrane.

340

341 **Interfacial interactions of endocytic condensates cause deformation of the cytosol and**
342 **membrane**

343

344 We hypothesized that free energy released by endocytic condensate phase separation is converted
345 into mechanical work to deform the membrane and the cytosol. This mechanical work is
346 manifested as an inward pressure on the membrane created by expansion of the condensate with
347 the requirement that volume of the condensate is conserved. Phenomena in which geometric
348 organization of matter is driven by the balances of opposing forces have been described for a range
349 of length scales and examples of these include “fingering instabilities” (Kull 1991, Hester 2008,
350 Xi, Byrnes et al. 2017).

351

352 The mechanics of CME can be described by analogy to a soft viscoelastic and sticky balloon bound
353 to a soft elastic sheet (Movie S2). If you were to press your finger into the center of the sheet-
354 balloon interface to create an invagination, the surface area of the balloon would have to increase
355 to maintain a constant volume and density of the balloon. Equally, if you were to grasp the sticky

356 surface of the balloon with your hands and pull outwards equally over the surface, except at the
357 elastic sheet-balloon interface, a tiny increase of the surface area would require a compensating
358 adjustment of the shape so that the balloon would maintain a constant volume. Since force would
359 be applied outwards everywhere except at the sheet balloon interface, it is there that an
360 invagination of the membrane-balloon interface would compensate for the pressure generated by
361 the outward force on the balloon surface.

362

363 In the case of CME, the grasping force is caused by interactions of molecules at the endocytic
364 condensate-cytoplasm interface. Balance between this binding and elastic/surface deformation
365 energies is achieved when the membrane invaginates. This idea is captured in a simple
366 phenomenological model expressed as the sum of mechanical strain energy (ϕ term) and work (ψ
367 term), respectively;

368

$$369 \quad U = \phi \cdot \delta^{1+\varepsilon} - \psi \cdot \delta ; \quad (1)$$

370

371 Here, U is a mean-field energy, δ is the invagination depth of both the membrane and cytosol
372 (which are coupled by virtue of conservation of volume of the condensate), and the exponent $\varepsilon >$
373 0 is determined by the deformation geometry (Methods). At equilibrium $\partial U/\partial \delta = 0$ and we expect
374 invagination to balance the two contributions such that δ^* minimizes energy in (1) resulting in,

375

$$376 \quad \delta^* = \left(\frac{\psi}{\phi (1 + \varepsilon)} \right)^{\frac{1}{\varepsilon}} ; \quad (2)$$

377

378 Equation (2) shows that the invagination depth δ is determined by the ratio ψ/ϕ and the deformation
379 geometry ε . To determine the numerical values of ϕ and ψ with mechanical contact theory, we
380 must estimate the geometries of the condensate, the viscoelastic properties of the cytosol, the
381 condensate and the membrane and from these values, determine the interfacial tensions among
382 them (Methods).

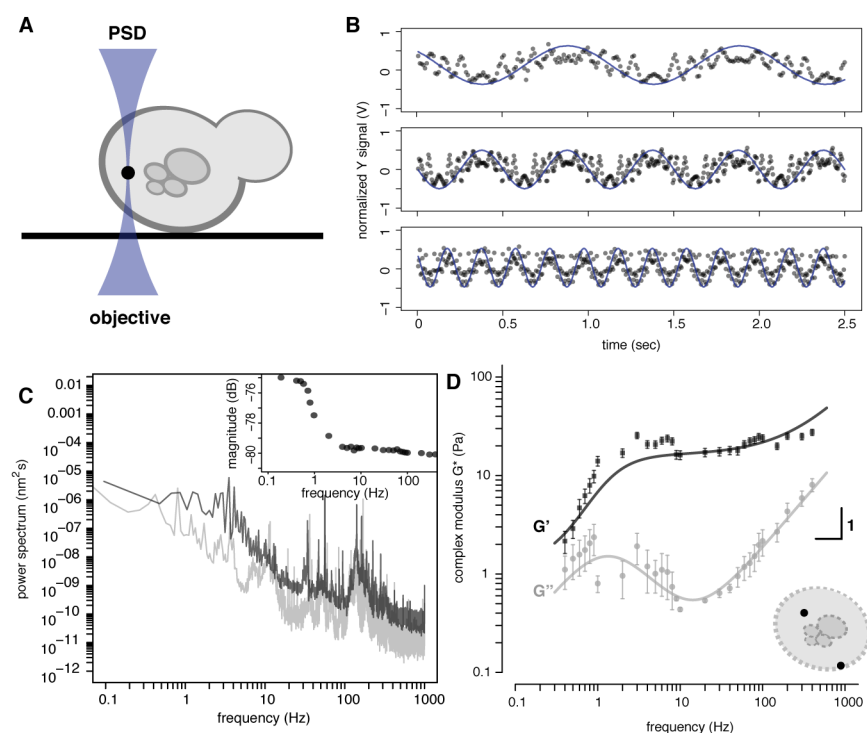
383

384 **Endocytic condensates are embedded in a viscoelastic cytosol**

385

386 We used active rheology to measure the material properties of the cytosol in which endocytic
387 condensates are embedded. We then calculated the condensate properties based on Hertz theory,
388 which directly relates the material properties of one elastic material to that of an embedded elastic
389 object, based on the deformation geometry, as described below. Specifically, we used optical
390 tweezers to examine the frequency-dependent amplitude and phase responses of polystyrene beads
391 embedded in cells (Figure 4A and Methods). Polystyrene beads of 200 nm diameter were
392 integrated into cells by osmoporation (Figure S4A-B). Measurements of passive diffusion of the
393 beads showed mean square displacements (MSD) close to that of random mechanical noise caused

394 by vibration of the microscope (Figure S4C). Furthermore, we established that the osmoporation
 395 procedure did not affect rheological properties of cells by measuring the MSD of expressed viral
 396 capsid microNS particles labeled with GFP in untreated or osmoporated cells and showing that
 397 their diffusion behaviors were identical (Figure S4D-F) (Munder, Midtvedt et al. 2016).
 398



399
 400
 401 **Figure 4 | Yeast cytosol is composed of a viscoelastic network of interacting proteins** (A) We used
 402 optical tweezers (beam between the microscope objective and a position sensitive detector (PSD) coupled
 403 to an acousto-optic device (AOD) to oscillate polystyrene beads in cells. Two pulses of osmotic shock were
 404 used to osmoporate 200 nm polystyrene beads (black) into Lat A-treated haploid yeast *GPD1Δ* cells. (B)
 405 PSD output signal in volts (V) as a function of time for acquisitions made at 1Hz (top), 2 Hz (middle) and
 406 5 Hz (bottom). A bead, located in the cell periphery, was oscillated with the AOD in the Y-axis of the
 407 specimen plane with fixed tweezer movement amplitude (normalized blue curve) at different frequencies.
 408 The recorded PSD raw traces (black points) were also normalized to a corresponding magnitude range
 409 (coherence cutoff of 0.9). (C) Power spectrum of the oscillated bead (black) with magnitude of response as
 410 a function of frequency (insert). (D) Decomposition of G^* as a function of frequency into G' (storage
 411 modulus; darker squares) and G'' (loss modulus; light shade circles) for beads distributed at both the cell
 412 periphery and interior (see schematic insert; mean \pm sd; $n = 17$ cells) with an average trap stiffness k_{trap} (mean
 413 \pm se; $8.0 \times 10^5 \pm 2.7 \times 10^5 \text{ N m}^{-1}$) and photodiode sensitivity factor β (mean \pm se; $10.7 \times 10^3 \pm 2.3 \times 10^3 \text{ nm}$
 414 V^{-1}). Data was fitted to a model of an entangled and crosslinked network of flexible polymers (Methods;
 415 Eq. 2.9-2.10). See also Figure S4.
 416

417 For active rheology experiments, we used an acousto-optic device to oscillate the position of the
 418 optical trap in the specimen plane at frequencies over four orders of magnitude and measured the
 419 displacement of trapped beads from the trap center using back focal plane interferometry (Figure
 420 4B). We thus measured the viscoelastic properties of the cytosol surrounding the beads by

421 measuring the phase and amplitude of displacements of beads in response to the oscillations of the
422 optical tweezers. Then, by calculating the power spectrum of unforced fluctuations of the bead,
423 we obtained storage (G') and loss (G'') moduli as a function of frequency (Figure 4C-D, S4G-H
424 and Methods) (Hendricks and Goldman 2017).

425
426 Cells and underlying structures show different mechanical properties depending on the rates at
427 which forces are applied to them (Hendricks, Holzbaur et al. 2012, Guo, Ehrlicher et al. 2013,
428 Guo, Ehrlicher et al. 2014). If a force is applied at a low velocity, the cell behaves like a viscous
429 fluid, flowing and taking on whatever shape it is forced into. When a force is applied at higher
430 velocity the material behaves like an elastic object, bouncing back to its original shape. As we
431 discuss below, these behaviors reflect the manner and strengths with which the molecules of the
432 material interact with each other and their environment.

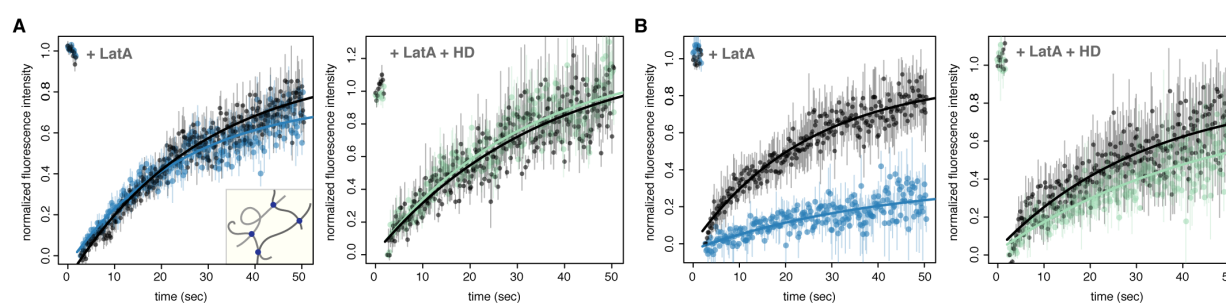
433
434 The material properties of the yeast cytoplasm and its interactions with the endocytic condensate
435 derive from the complex modulus *versus* frequency plot as follows (Figure 4D). When deformed
436 by the condensate growth (at a velocity of growth = 2360 ± 120 nm s⁻¹; corresponding to a stress
437 at $\sim 30 \pm 2$ Hz) the cytosol is elastic; membrane invagination occurs at a rate (a velocity of $7.4 \pm$
438 2.5 nm s⁻¹; corresponding to 0.1 ± 0.04 Hz) at which the cytoplasm is viscoelastic and very
439 compliant (Figure 4D and S4I-J). The G' and G'' we measured here in yeast are similar to those of
440 the cytoplasm of adherent mammalian cells (Hendricks, Holzbaur et al. 2012, Guo, Ehrlicher et al.
441 2013, Guo, Ehrlicher et al. 2014).

442
443 The material properties of the endocytic condensate were calculated using its geometric
444 dimensions (Figure 1B) and the material properties of the cytosol (Figure 4). As noted above,
445 classic Hertz theory relates contact geometries of elastic materials to their respective mechanical
446 properties. Therefore, we used the geometry of the endocytic condensates determined in our super-
447 resolution fluorescence imaging experiments and the moduli of the cytosol in which they are
448 embedded to estimate the endocytic condensate elastic modulus which was 59 Pa (Figure 1B, 4D,
449 and Methods; Eq. 3.7-3.10) (Hertz 1882). These results are consistent with protein condensates
450 that form elastic materials (Reichheld, Muiznieks et al. 2017) and suggests that endocytic
451 condensates have similar material properties as the surrounding cytosol, which has an elastic
452 modulus of 45 Pa at 1 Hz (Methods).

453
454 **PLD-containing coat proteins form a dense network of interacting molecules**

455
456 We estimated the average mesh size and permeability of the endocytic condensates by probing
457 them with fluorophore-conjugated dextran molecules of 2.4, 5.8, and 10.4 nm in diameter. We
458 measured FRAP and colocalization of these dextran molecules with either Sla1-mCherry or Syp1-
459 mCherry puncta (Figure 5 and S5). Although the density of 5.8 nm dextran-FITC is lower in Sla1
460 puncta than in the surrounding cytosol, the mobility of the 5.8 nm probe is equal in both regions

461 (Figure 5A and S5B-D). We observed that both 2.4 nm and 5.8 nm dextran-FITC recovered equally
462 well in the condensate and cytosolic zones (Figure 5A and S5F). In contrast, few 10.4 nm dextran-
463 FITC molecules permeate the PLD-rich protein network in the condensate, whereas they are
464 mobile in the neighboring cytosol (Figure 4B). When endocytic condensates are disrupted by
465 addition of 1,6-hexanediol, we observe equivalent mobility of 10.4 nm dextran-FITC between
466 cortical sites, labelled with the protein Syp1-mCherry, which is membrane-bound at cortical
467 patches in an HD-resistant manner, and neighboring cytosol (Figure 5 and S5E). These results are
468 consistent with an exclusion zone for ribosomes as discussed above and with exclusion of dextrans
469 by known protein-RNA phase separated condensates called P granules (Updike, Hachey et al.
470 2011, Wei, Elbaum-Garfinkle et al. 2017).
471



472
473

474 **Figure 5 | Porous meshwork structure of endocytic condensates is less permeable than cytosol (A)**
475 Fluorescence recovery after photobleaching (FRAP) of dextran-FITC probes within endocytic condensates
476 or neighbouring cytosol regions of interest. FRAP of the bleached 5.8 nm dextran-FITC within either a
477 Sla1-mCherry (left panel; Lat A treated cells; blue) or a Syp1-mCherry (right panel; Lat A and 5% HD
478 treated cells; green) puncta and neighbouring cytosol regions (black) without Sla1 or Syp1 signals
479 respectively. Insert is an illustration of a porous latticework composed of amorphous protein chains (grey
480 filaments) with binding sites (dots) through which they are non-covalently associated. (B) Same experiment
481 with 10.4 nm dextran-FITC that scarcely permeate the Sla1 puncta (left panel; Lat A treated cells; blue) but
482 are mobile when condensates are dissolved by HD (right panel; Lat A and 5% HD treated cells; green).
483 Data points (mean ± SEM; n = 10 cells) were fitted to a single term recovery function (Methods). See also
484 Figure S4.

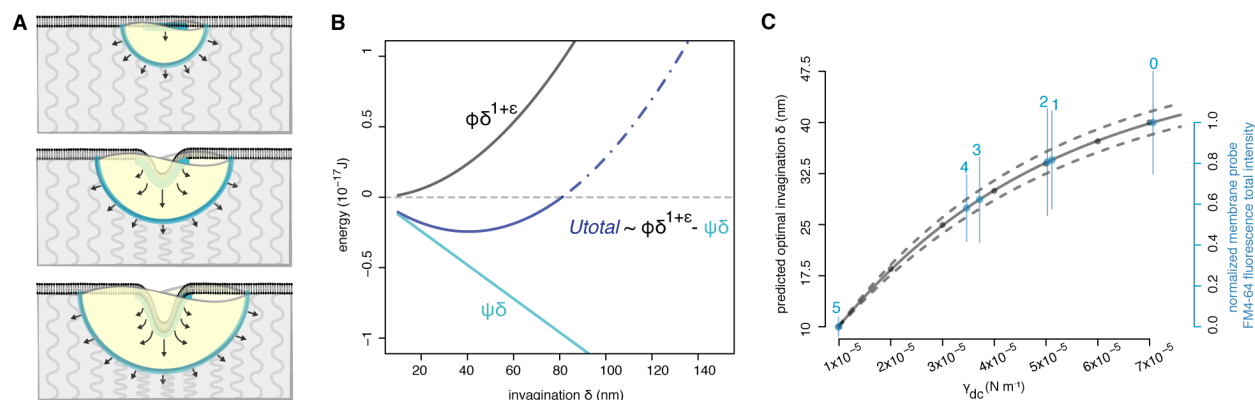
485

486 **Interactions of endocytic condensates with cytosol and membrane provide the required**
487 **energy to drive membrane invagination**

488

489 The deformation of the membrane in response to contact with a soft object depends on the
490 geometries and mechanical properties of the object and the vessel it is in (in our case the cytosol
491 of a cell) and the membrane (Figure 6A). Evidence from electron and super-resolution
492 fluorescence microscopy indicates that the favored geometry of the membrane is flat with an
493 invagination centered in the middle of the condensate (Figure 6A, lower). Such geometries are
494 explained by a local radial stress-gradient generated by the condensate adhesion to both the
495 membrane and cytosol or by local binding of adaptor proteins and distinct lipid compositions.

496 Simply stated, as the condensate grows, the interactions to the cytosol draws it inward and the
 497 membrane follows, mediated by its own interactions to the condensate and the requirement that
 498 the volume of the condensate be conserved.
 499



500
 501
502 Figure 6. Endocytic condensates do mechanical work to deform the membrane and cytosol (A)
 503 Illustration of a endocytic condensate (yellow) that binds to (wets) a bilayer membrane (black) and drives
 504 membrane invagination (top to bottom). Resultant membrane deformations reflect how forces balance
 505 under a Young-Dupré adhesion gradient (blue lines and arrows). Resistance to deformation is represented
 506 by grey curved lines. (B) Equation (1) (insert) was used to calculate the energy penalties (ϕ) and
 507 contributions (ψ) at the cytosol and membrane interfaces with the endocytic condensate. Total energy of
 508 the system (dark blue), energy penalties (black) and energy contributions (light blue) are presented as a
 509 function of membrane invagination (δ). The energy of membrane invagination is favourable for δ between
 510 about 15-80 nm (solid blue line) and unfavorable above 80 nm (dashed blue line). Quantities used to
 511 calculate energies are detailed in Figure S5, Table S3 and S4. (C) Our model predicts that vesicle size is
 512 proportional to the strength of condensate intermolecular protein-protein interactions that are proportional
 513 to γ_{dc} , the condensate-to-cytosol interfacial tension. Predicted membrane invagination δ as a function of γ_{dc}
 514 (left axis and black points). Data points were fitted to an exponential decay function (full line) with 95%
 515 confidence interval (dashed lines). Titration of 1,6-hexanediol was used to reduce intermolecular cohesion
 516 and therefore γ_{dc} resulting in reduced vesicle size as measured by uptake of the lipophilic membrane probe
 517 FM4-64 into *GPD1Δ Sla1-YFP* cells treated with Lat A (Right axis, red) versus % HD (blue numbers, n=
 518 25, mean \pm sd) expressed as a function of the condensate-cytosol interfacial tension γ_{dc} (Methods). See also
 519 Figure S5.

520
 521 We quantified the work performed by the condensate to invaginate the membrane using the storage
 522 and loss moduli obtained from the micro-rheology experiments, geometric data obtained from
 523 super-resolution imaging, and other data available from the literature. We used these values to
 524 solve the explicit form of the ϕ and ψ terms (mechanical strain and work, respectively) in Equation
 525 (1) as functions of membrane and cytosol invagination δ (Methods; Eq. 4.25-4.26). Using the
 526 Young-Laplace equation, we first estimated an interfacial tension for the condensate-cytosol
 527 interface to be approximately γ_{dc} of $7 \times 10^5 \text{ N}\cdot\text{m}^{-1}$. This estimate is based on the pressure difference
 528 across the cytosolic interface and the condensate mean curvature (Methods; Eq. 4.6). Our estimate
 529 for the interfacial tension falls within the range of values that have been reported for other protein

530 condensates, including nucleoli and P granules (Methods; Eq. 4.9) (Brangwynne, Mitchison et al.
531 2011, Elbaum-Garfinkle, Kim et al. 2015).

532

533 Given our estimates of γ_{dc} , we also determined the work of adhesion released when the condensate
534 surfaces are created, as described by the Young-Dupré equation (Figure 6 and Methods; Eq. 4.11).

535 We calculated an adhesion energy (ψ) of 4.9×10^{-18} J from interactions between the endocytic
536 condensate and both the membrane and cytosol (Figure 6B, S6 and Methods; Eq. 4.26). Our results

537 suggest that the most significant contribution of the mechanical energy comes from the
538 condensate-cytosol interface, where the adhesion energy of 2.9×10^{-18} J is enough to overcome an

539 energy penalty of 2.4×10^{-18} J to deform the membrane and the cytosol. This energy cost includes
540 the elastic, viscous, and interfacial stress penalties (Figure 6B, S6 and Table S4). We also

541 calculated an average adhesion energy of $1.3 \text{ kJ}\cdot\text{mol}^{-1}$ at the condensate-cytosol interface
542 (Methods), which is consistent with the free energies expected of non-covalent interactions

543 (Mahadevi and Sastry 2016).

544

545 Our model provides a physical framework to explain how endocytic condensates exert force to
546 induce invagination of membranes in actin-independent CME in our mutant yeast cells. The

547 interface between condensates, formed by phase separation of disordered proteins into cortical
548 bodies, and the cytosol or membrane deforms the surrounding materials through adhesive

549 interactions. Invagination occurs when ψ dominates ϕ in Equation (1) and is favored within the
550 observed δ interval of 40 nm to 80 nm (Figure S6). Notably, this predicted δ interval is within the

551 range of plasma membrane invagination of 70 nm or more, at which point membrane constriction
552 and vesicle scission mechanisms are activated to complete CME (Idrissi, Blasco et al. 2012).

553

554 **Condensate cohesion and interfacial tension determines the potential energy**

555

556 We propose that endocytic condensates store and dissipate mechanical energy in the form of
557 interfacial tension, whereby the composition of the condensates determine their interfacial

558 interactions, and provides the energy for adhesion and invagination of membranes. Accordingly,
559 the underlying energy stored within the condensates and the balance of interactions amongst

560 condensate components and solvent governs the interface. The effective potential energy ψ of
561 condensates, which is equivalent to the total work of adhesion, should be dictated by the density

562 and strengths of physical interactions amongst proteins within the condensate (the condensate
563 cohesion and interfacial tensions). We tested this hypothesis by using 1,6-hexanediol (HD) to

564 weaken the favorable free energies of the protein-protein interactions within condensates. These
565 interactions drive the phase separation of endocytic condensates, and HD titration would

566 correspond to a decrease of the condensate surface tension (γ_{dc} or ψ). Our model predicts that
567 invagination depth should vary continuously with ψ - Equation (2). We titrated HD below the

568 effective concentration that prevents protein phase separation and quantified individual membrane
569 excision events by measuring the uptake of the lipophilic membrane probe FM4-64 into cells by

570 fluorescence microscopy (Figure 2A and Methods). In Lat A treated *GPD1Δ* cells, our
571 measurement reports the amount of labeled membrane taken up into cells under the action of
572 endocytic condensates alone. By increasing subcritical HD concentration (corresponding to a
573 decrease in ψ), the average fluorescence-labeled membrane per vesicle (a proxy for invagination
574 δ) was continuously reduced over one order of magnitude in the value of γ_{dc} (Figure 6C and
575 Methods; Eq. 2.8). This observation fits with the reduced membrane invagination that we predicted
576 at the outset (*i.e.*, that δ scales with the ψ/ϕ ratio) when the condensate cohesion (γ_{dc} or ψ) is also
577 reduced (Figure 6C and Methods; Eq. 4.2).

578

579 Discussion

580 Existing models of actin-independent CME are implicit to our viscoelastic protein 581 condensate model

582

583 In the context of actin-independent CME in *S. cerevisiae*, we estimated that approximately $9.7 \times$
584 10^{-18} J of energy is required to produce an 80 nm deep membrane invagination. We have also
585 estimated that protein condensate formation generates 4.9×10^{-18} J to reach the energy minima
586 (Figure 6C and Table S4). This suggests that other curvature-generating mechanisms must provide
587 the energy balance to maintain or increase the profundity of the energy minimum in our model.
588 Several proposed mechanisms could provide significant sources of energy to account for this
589 deficit; such mechanisms may also depend on formation of the endocytic condensates. These
590 include (1), membrane curvature-inducing proteins and protein complexes, including convex-
591 shaped BAR (for Bin, Amphiphysin and Rvs) domain-containing proteins (Youn, Friesen et al.
592 2010, Yu and Schulten), (2), insertion of amphipathic protein helix into membrane (Ford, Mills et
593 al. 2002, Boucrot, Pick et al. 2012)(3), local relief of turgor pressure (Scher-Zagier and Carlsson
594 2016), (4), proteins that modulate lipid composition (Graham and Kozlov 2010, Anitei, Stange et
595 al. 2017) or (5), steric exclusion or crowding of proteins at cortical sites (Snead, Hayden et al.
596 2017). A counterargument to the latter point (5) is that calculations of the entropic gain and
597 pressure produced in the crowded protein layer, obtained with the Carnahan-Starling equation
598 which assumes that proteins are non-attracting (non-interacting) disks (Derganc and Copic 2016),
599 are not compatible with the interaction energies that we estimate to account for cohesion among
600 the condensate-forming proteins or adhesion at membrane and cytosol interfaces with the
601 condensate.

602

603 It is possible that most of these mechanisms have an additive effect *in vivo* and are integrated with
604 the condensate-based mechanism we introduce here to drive actin-independent CME. Binding of
605 Epsins (Ent1 and Ent2 proteins in yeast), in particular, has been proposed to facilitate deformation
606 of membranes by insertion of an amphipathic helix into the outer leaflet of the bilayer, which
607 pushes the head groups apart (Ford, Mills et al. 2002, Boucrot, Pick et al. 2012, Skruzny, Desfosses
608 et al. 2015). ENTH-containing Epsin proteins are also reported to reduce membrane tension of
609 artificial giant vesicles, thus facilitating deformation and curvature of the membrane (Gleisner,

610 Kroppen et al. 2016). By reducing the effective resistance of membrane elasticity, Epsin-
611 membrane interactions could shift right and increase the profundity of the energy minimum in our
612 model. At the same time, for these mechanisms to work, the proteins must be concentrated at
613 endocytic sites, a function served by their phase separation with the condensate.

614

615 **Implications of endocytic condensates to other emergent phenomena**

616

617 Our results provide a framework for answering many questions regarding CME and other
618 membrane budding processes. For example, given our observations, how is CME coupled to
619 signaling pathways that regulate vesicle formation? The PLD-containing CME proteins we
620 investigated are enriched for multiple phosphorylation sites, which undergo changes in response
621 to activation of a CME-regulating signaling pathway (Kanshin, Bergeron-Sandoval et al. 2015).
622 Since the amount and distribution of charge in disordered regions of proteins regulate their
623 interactions and conformations (Das and Pappu 2013), such post-translational modifications may
624 be important to regulating phase separation and material properties of CME condensates (Miao,
625 Tipakornsaowapak et al. 2018).

626

627 Our fluorescence microscopy and electron micrographic evidence from the literature suggests that
628 the endocytic condensate remains associated temporarily with mature vesicles (Kukulski, Schorb
629 et al. 2012). Does the condensate play any role in trafficking and fusing with, for instance, plasma
630 membrane (protein recycling) or lysosome (protein degradation)? CME also underlies several
631 fundamental mechanisms of vesicle trafficking and attendant membrane and vesicle protein cargo
632 transport, including late secretory pathways and neuronal synaptic vesicle recycling in which both
633 scission of budding vesicles and their re-fusion to other membranes occurs.

634

635 Yeast and human proteins implicated in clathrin-mediated vesicle trafficking are enriched for long
636 disordered protein domains (47 % of human and 23% of yeast proteins have long consecutive
637 disordered regions of up to or greater than 30 residues), whereas those involved in two other vesicle
638 trafficking systems are not (COPI: 8/5%; COPII: 8/5%) (Pietrosemoli, Panca et al. 2013). These
639 observations argue for investigating the generality and conservation of protein condensate
640 adhesion-driven membrane invagination as an underlying source of energy in clathrin-mediated
641 vesicle trafficking in the absence of actin polymerization.

642

643 Recent evidence suggests that neurodegenerative pathologies, such as Amyotrophic lateral
644 sclerosis, Huntington's and Alzheimer's, may result from both aberrant liquid-liquid phase
645 separation of proteins and disruption of endocytosis (Bhattacharyya, Banerjee et al. 2008, Wu and
646 Yao 2009, G. Liu, A.N. Coyne et al. 2017). In future work, it will be interesting to observe whether
647 adherent liquid-liquid phase separation of proteins in endocytic condensates contribute to these
648 pathologies.

649

650 Phase separation of proteins in an elastic network, such as yeast cytosol, is predicted to restrain
651 the size of condensates because condensates have a limited mechanical potential to deform the
652 cytosol in order to grow beyond the cytosol mesh size (Style, Sai et al. 2018). Our results suggest
653 that, beyond deformation of cellular structures, the material properties of the cytosol and the
654 interactions amongst proteins within the condensate can also dictate the dimensions of biopolymer
655 condensates found in cells.

656

657 Finally, it is possible that other liquid-liquid phase separated protein and protein nucleic acid
658 condensates influence cellular sub-structural dynamics and thus contribute to shaping cell, tissue,
659 and organism morphology (Bergeron-Sandoval, Safaee et al. 2016, Bauerlein, Saha et al. 2017,
660 Bergeron-Sandoval and Michnick 2018, Style, Sai et al. 2018). More broadly, interfacial contact
661 potentials between different biological materials may represent a vastly underestimated source of
662 complex pattern formation in biology, such as has been observed in embryonic tissue layers (Foty,
663 Pflieger et al. 1996), in a model of growing brain convolutions (Tallinen, Chung et al. 2016), in
664 protein stabilization (Gupta, Donlan et al. 2017) and in the ability of clathrin-coated structures to
665 wrap around and pinch collagen fibers (Elkhatib, Bresteau et al. 2017).

666 **Acknowledgements**

667 The authors acknowledge support from CIHR grants MOP-GMX-152556 (SWM), the US
668 National Institutes of Health grant R01NS056114 (RVP), the Fonds Québécois de la Recherche
669 sur la Nature et les Technologies (SWM and PF) and the Human Frontier Science Program
670 RGP0034/2017 (SWM and RVP). CEC was supported by the National Institute of General
671 Medical Sciences of the National Institutes of Health (NIH) under award T32GM008268. Research
672 in the Keller Lab is supported by National Science Foundation award MCB-1402059 to SLK. We
673 thank Cliff Brangwynne, David Drubin, Tom Pollard and Julien Berro for thoughtful discussion
674 and advice on the manuscript; Jackie Vogel for strains; Susan Liebman and Randal Halfmann for
675 plasmids; Jacqueline Kowarzyk and Philippe Garneau for technical assistance and Rosa Kaviani
676 for help with FRAP experiments.

677

678 **Author Contributions**

679 LPBS and SWM designed the research with the assistance of RVP; LPBS performed biological
680 research; LPBS, AJE, RVP and SWM analysed the biological data; CC, CEC and SLK performed
681 and analysed the vesicle leakage experiments; LPBS and HKH performed micro rheology
682 experiments; LPBS, HKH, AJE and AGH analysed micro rheology data; LPBS, HKH and PF
683 developed physical model; LPBS and SWM wrote the first version, all authors corrected the paper.

684

685 **Supplementary Materials**

686 Materials and Methods

687 Figures S1-S6

688 Tables S1-S4

689 Movies S1-S2

690 References

- 691 1. Aghamohammadzadeh, S. and K. R. Ayscough (2009). "Differential requirements for actin during yeast and
692 mammalian endocytosis." *Nat Cell Biol* **11**(8): 1039-1042.
- 693 2. Alberti, S., R. Halfmann, O. King, A. Kapila and S. Lindquist (2009). "A systematic survey identifies prions and
694 illuminates sequence features of prionogenic proteins." *Cell* **137**(1): 146-158.
- 695 3. Alberti, S., S. Saha, J. B. Woodruff, T. M. Franzmann, J. Wang and A. A. Hyman (2018). "A User's Guide for
696 Phase Separation Assays with Purified Proteins." *J Mol Biol*.
- 697 4. Anitei, M., C. Stange, C. Czupalla, C. Niehage, K. Schuhmann, P. Sala, A. Czogalla, T. Pursche, U. Coskun, A.
698 Shevchenko and B. Hoflack (2017). "Spatiotemporal Control of Lipid Conversion, Actin-Based Mechanical
699 Forces, and Curvature Sensors during Clathrin/AP-1-Coated Vesicle Biogenesis." *Cell Rep* **20**(9): 2087-2099.
- 700 5. Basu, R., E. L. Munteanu and F. Chang (2014). "Role of turgor pressure in endocytosis in fission yeast." *Mol*
701 *Biol Cell* **25**(5): 679-687.
- 702 6. Bauerlein, F. J. B., I. Saha, A. Mishra, M. Kalemanov, A. Martinez-Sanchez, R. Klein, I. Dudanova, M. S. Hipp,
703 F. U. Hartl, W. Baumeister and R. Fernandez-Busnadiego (2017). "In Situ Architecture and Cellular Interactions
704 of PolyQ Inclusions." *Cell* **171**(1): 179-187 e110.
- 705 7. Bergeron-Sandoval, L. P. and S. W. Michnick (2018). "Mechanics, Structure and Function of Biopolymer
706 Condensates." *J Mol Biol*.
- 707 8. Bergeron-Sandoval, L. P., N. Safae and S. W. Michnick (2016). "Mechanisms and Consequences of
708 Macromolecular Phase Separation." *Cell* **165**(5): 1067-1079.
- 709 9. Bhattacharyya, N. P., M. Banerjee and P. Majumder (2008). "Huntington's disease: roles of huntingtin-
710 interacting protein 1 (HIP-1) and its molecular partner HIPPI in the regulation of apoptosis and transcription."
711 *FEBS J* **275**(17): 4271-4279.
- 712 10. Boeke, D., S. Trautmann, M. Meurer, M. Wachsmuth, C. Godlee, M. Knop and M. Kaksonen (2014).
713 "Quantification of cytosolic interactions identifies Ed1 oligomers as key organizers of endocytosis." *Mol Syst*
714 *Biol* **10**: 756.
- 715 11. Boucrot, E., A. Pick, G. Camdere, N. Liska, E. Evergren, H. T. McMahon and M. M. Kozlov (2012). "Membrane
716 fission is promoted by insertion of amphipathic helices and is restricted by crescent BAR domains." *Cell* **149**(1):
717 124-136.
- 718 12. Brangwynne, C. P., C. R. Eckmann, D. S. Courson, A. Rybarska, C. Hoegge, J. Gharakhani, F. Julicher and A. A.
719 Hyman (2009). "Germline P granules are liquid droplets that localize by controlled dissolution/condensation."
720 *Science* **324**(5935): 1729-1732.
- 721 13. Brangwynne, C. P., T. J. Mitchison and A. A. Hyman (2011). "Active liquid-like behavior of nucleoli determines
722 their size and shape in *Xenopus laevis* oocytes." *Proc Natl Acad Sci U S A* **108**(11): 4334-4339.
- 723 14. Carlsson, A. E. and P. V. Bayly (2014). "Force generation by endocytic actin patches in budding yeast." *Biophys*
724 *J* **106**(8): 1596-1606.
- 725 15. Conner, S. D. and S. L. Schmid (2003). "Regulated portals of entry into the cell." *Nature* **422**(6927): 37-44.
- 726 16. Darwin, C. (1859). On the origin of species by means of natural selection, or, The preservation of favoured races
727 in the struggle for life. London, J. Murray.
- 728 17. Das, R. K. and R. V. Pappu (2013). "Conformations of intrinsically disordered proteins are influenced by linear
729 sequence distributions of oppositely charged residues." *Proc Natl Acad Sci U S A* **110**(33): 13392-13397.
- 730 18. Derganc, J. and A. Copic (2016). "Membrane bending by protein crowding is affected by protein lateral
731 confinement." *Biochim Biophys Acta* **1858**(6): 1152-1159.
- 732 19. Elbaum-Garfinkle, S., Y. Kim, K. Szczepaniak, C. C. Chen, C. R. Eckmann, S. Myong and C. P. Brangwynne
733 (2015). "The disordered P granule protein LAF-1 drives phase separation into droplets with tunable viscosity
734 and dynamics." *Proc Natl Acad Sci U S A* **112**(23): 7189-7194.
- 735 20. Elkhatib, N., E. Bresteau, F. Baschieri, A. L. Rioja, G. van Niel, S. Vassilopoulos and G. Montagnac (2017).
736 "Tubular clathrin/AP-2 lattices pinch collagen fibers to support 3D cell migration." *Science* **356**(6343).
- 737 21. Feric, M., N. Vaidya, T. S. Harmon, D. M. Mitrea, L. Zhu, T. M. Richardson, R. W. Kriwacki, R. V. Pappu and
738 C. P. Brangwynne (2016). "Coexisting Liquid Phases Underlie Nucleolar Subcompartments." *Cell* **165**(7): 1686-
739 1697.
- 740 22. Ford, M. G., I. G. Mills, B. J. Peter, Y. Vallis, G. J. Praefcke, P. R. Evans and H. T. McMahon (2002). "Curvature
741 of clathrin-coated pits driven by epsin." *Nature* **419**(6905): 361-366.
- 742 23. Foty, R. A., C. M. Pflieger, G. Forgacs and M. S. Steinberg (1996). "Surface tensions of embryonic tissues predict
743 their mutual envelopment behavior." *Development* **122**(5): 1611-1620.
- 744 24. G. Liu, A.N. Coyne, F. Pei, S. Vaughan, M. Chung, D. C. Zarnescu and J. R. Buchan (2017). "Endocytosis

- 745 regulates TDP-43 toxicity and turnover." *Nature communications* **8**(2092).
- 746 25. Gleisner, M., B. Kroppen, C. Fricke, N. Teske, T. T. Kliesch, A. Janshoff, M. Meinecke and C. Steinem (2016).
- 747 "Epsin N-terminal Homology Domain (ENTH) Activity as a Function of Membrane Tension." *J Biol Chem*
- 748 **291**(38): 19953-19961.
- 749 26. Graham, T. R. and M. M. Kozlov (2010). "Interplay of proteins and lipids in generating membrane curvature."
- 750 *Curr Opin Cell Biol* **22**(4): 430-436.
- 751 27. Guo, M., A. J. Ehrlicher, M. H. Jensen, M. Renz, J. R. Moore, R. D. Goldman, J. Lippincott-Schwartz, F. C.
- 752 Mackintosh and D. A. Weitz (2014). "Probing the stochastic, motor-driven properties of the cytoplasm using
- 753 force spectrum microscopy." *Cell* **158**(4): 822-832.
- 754 28. Guo, M., A. J. Ehrlicher, S. Mahammad, H. Fabich, M. H. Jensen, J. R. Moore, J. J. Fredberg, R. D. Goldman
- 755 and D. A. Weitz (2013). "The role of vimentin intermediate filaments in cortical and cytoplasmic mechanics."
- 756 *Biophys J* **105**(7): 1562-1568.
- 757 29. Gupta, K., J. A. Donlan, J. T. Hopper, P. Uzdaviny, M. Landreh, W. B. Struwe, D. Drew, A. J. Baldwin, P. J.
- 758 Stansfeld and C. V. Robinson (2017). "The role of interfacial lipids in stabilizing membrane protein oligomers."
- 759 *Nature* **541**(7637): 421-424.
- 760 30. Hendricks, A. G. and Y. E. Goldman (2017). "Measuring Molecular Forces Using Calibrated Optical Tweezers
- 761 in Living Cells." *Methods Mol Biol* **1486**: 537-552.
- 762 31. Hendricks, A. G., E. L. Holzbaur and Y. E. Goldman (2012). "Force measurements on cargoes in living cells
- 763 reveal collective dynamics of microtubule motors." *Proc Natl Acad Sci U S A* **109**(45): 18447-18452.
- 764 32. Hertz, H. R. (1882). *Ueber die Beruehrung elastischer Koerper (On Contact Between Elastic Bodies)*. Leipzig,
- 765 Germany, 1895.
- 766 33. Hester, J. J. (2008). "The Crab Nebula: An astrophysical chimera." *Annual Review of Astronomy and*
- 767 *Astrophysics* **46**: 127-155.
- 768 34. Holland, D. O. and M. E. Johnson (2018). "Stoichiometric balance of protein copy numbers is measurable and
- 769 functionally significant in a protein-protein interaction network for yeast endocytosis." *PLoS Comput Biol* **14**(3):
- 770 e1006022.
- 771 35. Idrissi, F. Z., A. Blasco, A. Espinal and M. I. Geli (2012). "Ultrastructural dynamics of proteins involved in
- 772 endocytic budding." *Proc Natl Acad Sci U S A* **109**(39): E2587-2594.
- 773 36. Kanshin, E., L. P. Bergeron-Sandoval, S. S. Isik, P. Thibault and S. W. Michnick (2015). "A cell-signaling
- 774 network temporally resolves specific versus promiscuous phosphorylation." *Cell Rep* **10**(7): 1202-1214.
- 775 37. Khan, T., T. S. Kandola, J. Wu, S. Venkatesan, E. Ketter, J. J. Lange, A. Rodriguez Gama, A. Box, J. R. Unruh,
- 776 M. Cook and R. Halfmann (2018). "Quantifying Nucleation In Vivo Reveals the Physical Basis of Prion-like
- 777 Phase Behavior." *Mol Cell* **71**(1): 155-168 e157.
- 778 38. Khurana, R., C. Coleman, C. Ionescu-Zanetti, S. A. Carter, V. Krishna, R. K. Grover, R. Roy and S. Singh
- 779 (2005). "Mechanism of thioflavin T binding to amyloid fibrils." *J Struct Biol* **151**(3): 229-238.
- 780 39. Kroschwald, S., S. Maharana, D. Mateju, L. Malinowska, E. Nuske, I. Poser, D. Richter and S. Alberti (2015).
- 781 "Promiscuous interactions and protein disaggregases determine the material state of stress-inducible RNP
- 782 granules." *Elife* **4**: e06807.
- 783 40. Kukulski, W., M. Schorb, M. Kaksonen and J. A. Briggs (2012). "Plasma membrane reshaping during
- 784 endocytosis is revealed by time-resolved electron tomography." *Cell* **150**(3): 508-520.
- 785 41. Kull, H. J. (1991). "Theory of the Rayleigh-Taylor Instability." *Physics Reports-Review Section of Physics*
- 786 *Letters* **206**(5): 197-325.
- 787 42. Li, D., L. Shao, B. C. Chen, X. Zhang, M. Zhang and B. Moses (2015). "Extended-resolution structured
- 788 illumination imaging of endocytic and cytoskeletal dynamics." *Science (New York, NY)*.
- 789 43. Li, X. H., P. L. Chavali, R. Pancsa, S. Chavali and M. M. Babu (2018). "Function and Regulation of Phase-
- 790 Separated Biological Condensates." *Biochemistry*.
- 791 44. Li, Y., R. Lipowsky and R. Dimova (2011). "Membrane nanotubes induced by aqueous phase separation and
- 792 stabilized by spontaneous curvature." *Proc Natl Acad Sci U S A* **108**(12): 4731-4736.
- 793 45. Lin, Y., D. S. W. Protter, M. K. Rosen and R. Parker (2015). "Formation and Maturation of Phase-Separated
- 794 Liquid Droplets by RNA-Binding Proteins." *Molecular Cell* **60**(2): 208-219.
- 795 46. Mahadevi, A. S. and G. N. Sastry (2016). "Cooperativity in Noncovalent Interactions." *Chem Rev* **116**(5): 2775-
- 796 2825.
- 797 47. Malinowska, L., S. Kroschwald and S. Alberti (2013). "Protein disorder, prion propensities, and self-organizing
- 798 macromolecular collectives." *Biochim Biophys Acta* **1834**(5): 918-931.
- 799 48. Miao, Y., T. Tipakornsaowapak, L. Zheng, Y. Mu and E. Lewellyn (2018). "Phospho-regulation of intrinsically
- 800 disordered proteins for actin assembly and endocytosis." *FEBS J*.

- 801 49. Molliex, A., J. Temirov, J. Lee, M. Coughlin, A. P. Kanagaraj, H. J. Kim, T. Mittag and J. P. Taylor (2015).
802 "Phase separation by low complexity domains promotes stress granule assembly and drives pathological
803 fibrillization." *Cell* **163**(1): 123-133.
- 804 50. Mukherjee, D., B. G. Coon, D. F. Edwards, 3rd, C. B. Hanna, S. A. Longhi, J. M. McCaffery, B. Wendland, L.
805 A. Retegui, E. Bi and R. C. Aguilar (2009). "The yeast endocytic protein Epsin 2 functions in a cell-division
806 signaling pathway." *J Cell Sci* **122**(Pt 14): 2453-2463.
- 807 51. Mund, M., J. A. van der Beek, J. Deschamps, S. Dmitrieff, J. L. Monster, A. Picco, F. Nedelec, M. Kaksonen
808 and J. Ries (2017). "Systematic analysis of the molecular architecture of endocytosis reveals a nanoscale actin
809 nucleation template that drives efficient vesicle formation." *bioRxiv*.
- 810 52. Munder, M. C., D. Midtvedt, T. Franzmann, E. Nuske, O. Otto, M. Herbig, E. Ulbricht, P. Muller, A.
811 Taubenberger, S. Maharana, L. Malinowska, D. Richter, J. Guck, V. Zaburdaev and S. Alberti (2016). "A pH-
812 driven transition of the cytoplasm from a fluid- to a solid-like state promotes entry into dormancy." *Elife* **5**.
- 813 53. Pappu, R. V., X. Wang, A. Vitalis and S. L. Crick (2008). "A polymer physics perspective on driving forces and
814 mechanisms for protein aggregation." *Arch Biochem Biophys* **469**(1): 132-141.
- 815 54. Peskett, T. R., F. Rau, J. O'Driscoll, R. Patani, A. R. Lowe and H. R. Saibil (2018). "A Liquid to Solid Phase
816 Transition Underlying Pathological Huntingtin Exon1 Aggregation." *Mol Cell* **70**(4): 588-601 e586.
- 817 55. Pietrosemoli, N., R. Pancsa and P. Tompa (2013). "Structural disorder provides increased adaptability for vesicle
818 trafficking pathways." *PLoS Comput Biol* **9**(7): e1003144.
- 819 56. Reichheld, S. E., L. D. Muiznieks, F. W. Keeley and S. Sharpe (2017). "Direct observation of structure and
820 dynamics during phase separation of an elastomeric protein." *Proc Natl Acad Sci U S A* **114**(22): E4408-E4415.
- 821 57. Scher-Zagier, J. K. and A. E. Carlsson (2016). "Local Turgor Pressure Reduction via Channel Clustering."
822 *Biophys J* **111**(12): 2747-2756.
- 823 58. Skruzny, M., T. Brach, R. Ciuffa, S. Rybina, M. Wachsmuth and M. Kaksonen (2012). "Molecular basis for
824 coupling the plasma membrane to the actin cytoskeleton during clathrin-mediated endocytosis." *Proc Natl Acad*
825 *Sci U S A* **109**(38): E2533-2542.
- 826 59. Skruzny, M., A. Desfosses, S. Prinz, S. O. Dodonova, A. Gieras, C. Uetrecht, A. J. Jakobi, M. Abella, W. J. H.
827 Hagen, J. Schulz, R. Meijers, V. Rybin, J. A. G. Briggs, C. Sachse and M. Kaksonen (2015). "An Organized Co-
828 assembly of Clathrin Adaptors Is Essential for Endocytosis." *Developmental Cell* **33**(2): 150-162.
- 829 60. Snead, W. T., C. C. Hayden, A. K. Gadok, C. Zhao, E. M. Lafer, P. Rangamani and J. C. Stachowiak (2017).
830 "Membrane fission by protein crowding." *Proc Natl Acad Sci U S A* **114**(16): E3258-E3267.
- 831 61. Sochacki, K. A., A. M. Dickey, M. P. Strub and J. W. Taraska (2017). "Endocytic proteins are partitioned at the
832 edge of the clathrin lattice in mammalian cells." *Nat Cell Biol* **19**(4): 352-361.
- 833 62. Style, R. W., T. Q. Sai, N. Fanelli, M. Ijavi, K. Smith-Mannschott, Q. Xu, L. A. Wilen and E. R. Dufresne (2018).
834 "Liquid-Liquid Phase Separation in an Elastic Network." *Physical Review X* **8**(1).
- 835 63. Tallinen, T., J. Chung, F. Rousseau, N. Girard, J. Lefèvre and L. Mahadevan (2016). "On the growth and form
836 of cortical convolutions." *Nature Physics* **12**: 588-593.
- 837 64. Tang, H. Y., J. Xu and M. Cai (2000). "Pan1p, End3p, and Sla1p, three yeast proteins required for normal
838 cortical actin cytoskeleton organization, associate with each other and play essential roles in cell wall
839 morphogenesis." *Mol Cell Biol* **20**(1): 12-25.
- 840 65. Thompson, D. A. W. (1917). *On growth and form*. Cambridge Eng., University press.
- 841 66. Toombs, J. A., B. R. McCarty and E. D. Ross (2009). "Compositional Determinants of Prion Formation in Yeast."
842 *Molecular and Cellular Biology* **30**(1): 319-332.
- 843 67. Updike, D. L., S. J. Hachey, J. Kreher and S. Strome (2011). "P granules extend the nuclear pore complex
844 environment in the *C. elegans* germ line." *J Cell Biol* **192**(6): 939-948.
- 845 68. Wang, J., J. M. Choi, A. S. Holehouse, H. O. Lee, X. Zhang, M. Jahnel, S. Maharana, R. Lemaitre, A.
846 Pozniakovsky, D. Drechsel, I. Poser, R. V. Pappu, S. Alberti and A. A. Hyman (2018). "A Molecular Grammar
847 Governing the Driving Forces for Phase Separation of Prion-like RNA Binding Proteins." *Cell*.
- 848 69. Warren, D. T., P. D. Andrews, C. W. Gourlay and K. R. Ayscough (2002). "Sla1p couples the yeast endocytic
849 machinery to proteins regulating actin dynamics." *J Cell Sci* **115**(Pt 8): 1703-1715.
- 850 70. Wei, M.-T., S. Elbaum-Garfinkle, A. S. Holehouse, C. C.-H. Chen, M. Feric, C. B. Arnold, R. D. Priestley, R.
851 V. Pappu and C. P. Brangwynne (2017). "Phase behaviour of disordered proteins underlying low density and
852 high permeability of liquid organelles." *NATURE CHEMISTRY*.
- 853 71. Weirich, K. L., S. Banerjee, K. Dasbiswas, T. A. Witten, S. Vaikuntanathan and M. L. Gardel (2017). "Liquid
854 behavior of cross-linked actin bundles." *Proc Natl Acad Sci U S A* **114**(9): 2131-2136.
- 855 72. Wu, F. and P. J. Yao (2009). "Clathrin-mediated endocytosis and Alzheimer's disease: an update." *Ageing Res*
856 *Rev* **8**(3): 147-149.

- 857 73. Xi, K., T. Byrnes and H. Saito (2017). "Fingering instabilities and pattern formation in a two-component dipolar
858 Bose-Einstein condensate." [arXiv 1704.04949v1](#)
- 859 74. Youn, J. Y., H. Friesen, T. Kishimoto, W. M. Henne, C. F. Kurat, W. Ye, D. F. Ceccarelli, F. Sicheri, S. D.
860 Kohlwein, H. T. McMahon and B. J. Andrews (2010). "Dissecting BAR domain function in the yeast
861 Amphiphysins Rvs161 and Rvs167 during endocytosis." *Mol Biol Cell* **21**(17): 3054-3069.
- 862 75. Yu, H. and K. Schulten (2013). "Membrane sculpting by F-BAR domains studied by molecular dynamics
863 simulations." *PLoS Comput Biol* **9**(1): e1002892.
- 864